



Universiteit
Leiden
The Netherlands

Advancing surgical guidance: from (hybrid) molecule to man and beyond
Berg, N.S. van den

Citation

Berg, N. S. van den. (2016, November 10). *Advancing surgical guidance: from (hybrid) molecule to man and beyond*. Retrieved from <https://hdl.handle.net/1887/44147>

Version: Not Applicable (or Unknown)

License: [Licence agreement concerning inclusion of doctoral thesis in the Institutional Repository of the University of Leiden](#)

Downloaded from: <https://hdl.handle.net/1887/44147>

Note: To cite this publication please use the final published version (if applicable).

Cover Page



Universiteit Leiden



The handle <http://hdl.handle.net/1887/44147> holds various files of this Leiden University dissertation

Author: Berg, Nynke van den

Title: Advancing surgical guidance : from (hybrid) molecule to man and beyond

Issue Date: 2016-11-10



CHAPTER

2

FLUORESCENCE GUIDANCE IN UROLOGIC SURGERY

Adapted from: van den Berg NS, van Leeuwen FWB and van der Poel HG. Curr Opin Urol. 2012;22:109-20.

ABSTRACT

Fluorescent tracers can provide anatomical and functional information without altering the visual surgical field. Despite the advances that are being made in tracer development, only a few fluorescent tracers are available for urological interventions. Protoporphyrin IX, hypericin, fluorescein, and indocyanine green were shown to facilitate surgical resection in various ways. Hybrid imaging agents, combining radio- and fluorescent labels, have shown improved integration between preoperative and intraoperative imaging. With the rise of surgical fluorescence guidance, various camera systems have been developed that are tailored for optimal detection of the fluorochromes of interest. In this review, the basics of fluorescence-guided surgery, including tracer and hardware requirements are discussed.

INTRODUCTION

Surgical performance is partly dependent on functional preoperative imaging, such as single photon emission computed tomography combined with computed tomography (SPECT/CT) or positron emission tomography (PET), to identify local areas of interest. Preoperative imaging may reveal anatomical details on organ orientation, and in some cases tumor location, but is often poorly translated into the surgical field. Intraoperative guidance so far is mainly limited to visual anatomical landmarks such as vessels and bones. Functional imaging information would therefore be a useful addition during surgical procedures. Intraoperatively, the gamma-ray detection probe (hereafter referred to as gamma probe) allows for radiotracer detection in for example sentinel nodes (SNs) based on acoustic tracing, but suffers from a background signal emitted from the injection site [1]. Moreover, depth perception is hampered due to collimation issues [1]. As such this technology alone does not allow for detection with a high spatial resolution. Ideally, functional information would be integrated into a visual image during surgery. Fluorescent tracers possess several properties that make them interesting candidates for functional imaging; most importantly they can be imaged in real-time within the surgical field without contaminating this field. To date, several approaches have been explored to achieve intraoperative fluorescence guidance. However, the clinical introduction of fluorescent tracers, and in particular for urological applications, is still in its infancy, though rapidly emerging. In this review, the basics of fluorescence-guided surgery, including tracer development and hardware requirements are discussed focusing on the field of urology.

EXOGENOUS FLUORESCENT TRACERS

Fluorescence imaging differs markedly from the visual detection of the more common vital dyes such as methylene blue and patent blue. Blue dye visualization is a result of light absorbance, which is maximal in the visual range (400-650 nm) and minimal in the near-infrared range (700-1000 nm), whereas fluorescence is based on light emission by fluorochromes. For more in-depth information regarding the basics of fluorescence, please see supporting information. Despite the advances that are being made in tracer development, only a few exogenous fluorescent tracers are available for urologic interventions. Currently only protoporphyrin IX (PpIX) precursors 5-aminolevulinic acid (5-ALA) and hexylaminolevulinate (HAL), fluorescein and indocyanine green (ICG) have received approval for clinical use by the Food and Drug Administration (FDA; Table 1, Figure 1). Several newly developed fluorescent tracers, though not FDA approved yet, have already been studied in a urological setting, such as hypericin and the hybrid tracer ICG-^{99m}Tc-nanocolloid (Table 1, Figure 1).

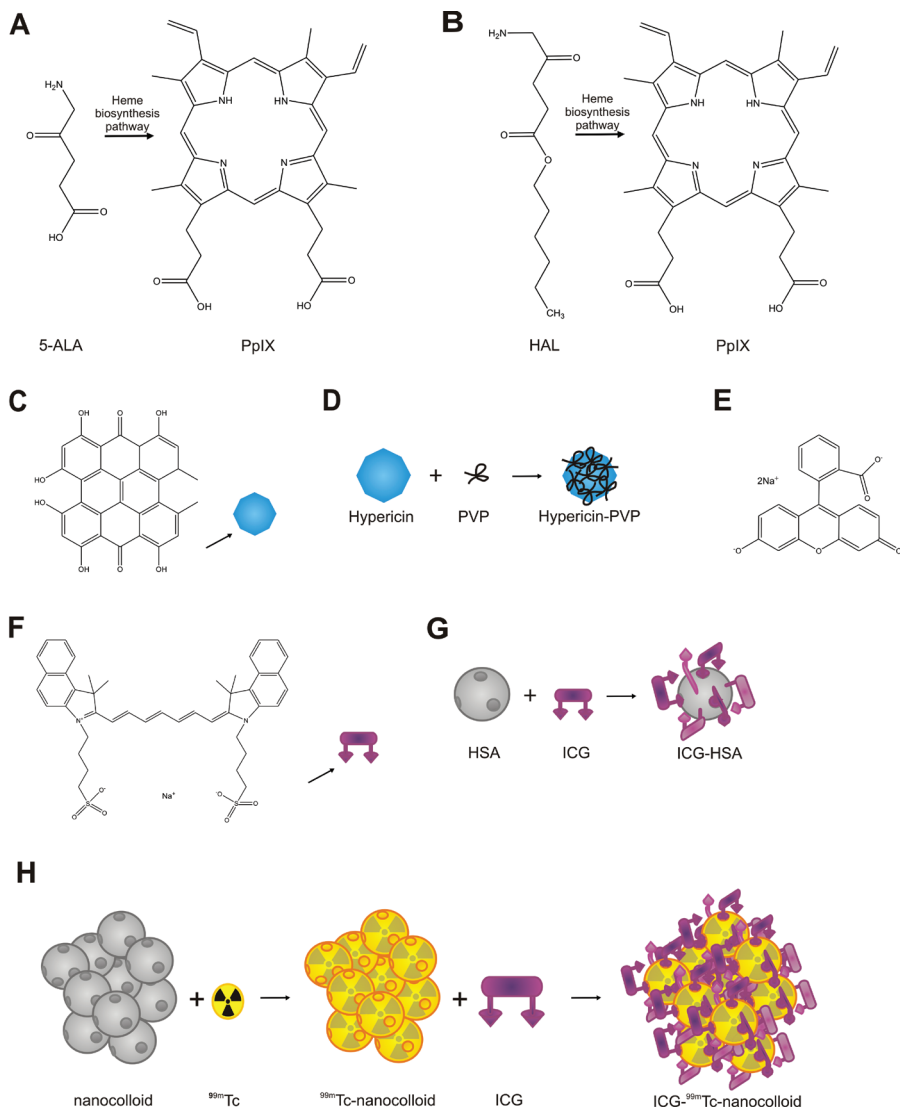


Figure 1. Structures of clinically available fluorescent tracers. A) 5-ALA and B) HAL are metabolically converted in the red fluorescing protoporphyrin IX (PpIX) during the initial steps of the heme biosynthesis pathway; C) Hypericin; D) Mixing hypericin with PVP results in water-soluble hypericin-PVP; E) Fluorescein; F) ICG; G) Formation of ICG-HSA; and H) Schematic overview of the assembly of the hybrid tracer ICG-^{99m}Tc-nanocolloid. Nanocolloid

(HSA aggregate) and ^{99m}Tc covalently bind, thereby forming ^{99m}Tc-nanocolloid. Via non-covalent self-assembly, ICG-^{99m}Tc-nanocolloid is formed when mixing ^{99m}Tc-nanocolloid and ICG. 5-ALA = 5-aminolevulinic acid; HAL = hexylamino-levulinate; HSA = human serum albumin; ICG = indocyanine green; PpIX = protoporphyrin IX; PVP = polyvinylpyrrolidone; Na = sodium; Tc = technetium.

Table 1. Clinically available exogenous fluorescence tracers

Tracer	Excitation and emission peaks	QY	Target	Urological imaging application
<i>Clinically approved</i>				
PpIX	$\lambda_{\text{ex max}}$ 450 nm; $\lambda_{\text{em max}}$ 635 nm	0.011	Heme biosynthesis pathway; accumulation in tumor cells (mainly used for PDD and PDT)	Detection of bladder [2-6,7-11], prostate [12-15], and penile lesions [16,17]
Fluorescein	$\lambda_{\text{ex max}}$ 488 nm; $\lambda_{\text{em max}}$ 530 nm	0.76	Accumulation near/around tumor cells	Bladder carcinoma [18,19] and renal vasculature and tumor [20] detection
ICG	$\lambda_{\text{ex max}}$ 780 nm; $\lambda_{\text{em max}}$ 820-830 nm	0.0028	Lymphatic and vascular system and urinary tract	Ureter [21] and vasculature [22] visualization
<i>Clinically evaluated</i>				
Hypericin	$\lambda_{\text{ex max}}$ 598 nm; $\lambda_{\text{em max}}$ 649 nm	<0.02	Tumor cell accumulation	Detection of bladder carcinoma [23-25]
Hypericin-PVP	$\lambda_{\text{ex max}}$ 595 nm; $\lambda_{\text{em max}}$ 651 nm	-	Tumor cell accumulation	Detection of bladder carcinoma [26]
ICG- ^{99m} Tc-nanocolloid	$\lambda_{\text{ex max}}$ 807 nm; $\lambda_{\text{em max}}$ 822 nm	-	Lymph nodes	SN biopsy procedure prostate cancer [1,2]

QY = quantum yield; $\lambda_{\text{ex max}}$ = excitation maximum; $\lambda_{\text{em max}}$ = emission maximum; PpIX = protoporphyrin IX; PDD = photodynamic diagnosis; PDT = photodynamic therapy; ICG = indocyanine green; Tc = technetium; NADH = nicotinamide adenine dinucleotide hydrogen; PVP = polyvinylpyrrolidone; SN = sentinel node.

PROTOPORPHYRIN IX

5-ALA (LEVULAN, DUSA Pharmaceuticals Inc., Wilmington, Massachusetts, USA; Figure 1A), a non-fluorescent prodrug, is the first compound in the heme biosynthesis pathway and is enzymatically converted into the fluorescent PpIX (Figure 1A) and finally into heme in the mitochondria. After 5-ALA administration, the abundantly produced PpIX cannot be rapidly converted into heme and will therefore accumulate intracellularly, leading to a higher signal intensity in proliferative (tumor) tissue [28]. Decreased activity of the enzyme ferrochelatase, which is responsible for the conversion of PpIX into heme and limited availability of iron have been shown to contribute to increased PpIX accumulation in tumor cells [28]. Porphyrins, such as PpIX, have been well studied for their application as photosensitizers for photodynamic diagnosis and -therapy (PDD and PDT, respectively) of cancer [29]. When excited with ultraviolet light, PpIX had a visual red fluorescence emission ($\lambda_{\text{ex max}}$: 450 nm; $\lambda_{\text{em max}}$: 635 nm; quantum yield 0.011 in water [29, 30]), which does not necessarily give the best contrast during urological applications; the tissue background is generally also reddish. However, on a white background, such as bladder mucosa, this red fluorescence may provide sufficient contrast for surgical guidance.

5-ALA can be administered orally, intravenously or can be intravesically instilled into the bladder. In a prospective randomized comparison of intravesical 5-ALA instillation for the early detection of small bladder tumors by cystoscopy, Stenzl et al. [10] showed that although slightly more patients in the 5-ALA arm were diagnosed with bladder lesions, the recurrence-free and progression-free survival at 12 months did not significantly differ from the placebo group. These findings are contradictory to earlier data from other groups [2-5] who reported a benefit of PpIX-guided cystoscopy for bladder cancer detection. Inexperience with fluoroscopy, a low number of carcinoma in situ patients, and more meticulous inspection in the placebo group were put forward as explanations for a lack of benefit for fluorescence-guided cystoscopy found in their study [10].

Additionally, 5-ALA has also been used for the detection of penile (Figure 2A) and prostate cancer. Local application of 5-ALA provided fluorescence guidance for the identification and resection of penile carcinoma [16,17]. Zaak et al. [15] showed accumulation of PpIX in prostate cancer tumor cells in 16 out of 16 patients following oral administration of 5-ALA. Moreover, two small multi-institutional phase II nonrandomized studies (n=24 and n=39) showed that oral 5-ALA administration (20 mg/kg), 3 h prior to surgery, might be useful for the intraoperative detection of a positive surgical margin during prostatectomy [12,14]. In a Japanese study (n=16), the specificity and sensitivity for detecting a positive margin during prostatectomy were 82 and 69%, respectively [13].

Both the cellular uptake of 5-ALA and the fluorescence quantum yield of PpIX are limited, which has led to the development of a great number of alternative structures based on the same principle [29]. Already clinically approved and used is HAL (HEXVIX; Photocure, Oslo, Norway; Figure 1B), which was obtained by addition of a lipophilic hexyl moiety to 5-ALA. HAL is considered to be superior to 5-ALA with respect to fluorescence intensity (a 2-4 times higher intensity was reported using a lower dose and a shorter incubation time), pharmacokinetic properties, and ease of preparation [11,29]. Recent studies found a benefit for fluorescence cystoscopy after bladder instillation of HAL over white light cystoscopy, in detecting carcinoma in situ of the bladder (87 vs. 75%) following bladder instilled HAL [7], but also for the management of multifocal recurrent non-muscle invasive bladder cancer [9]. Moreover, Ray et al. [8] showed improved bladder cancer diagnosis in patients previously treated with bacilli Calmette-Guèrin (Figure 2B). A reduced recurrence rate was reported following HAL fluorescence-guided transurethral resection of the bladder (TURB) as compared to conventional white light TURB (31 vs. 47%) [6].

For the detection of bladder cancer, especially carcinoma in situ, both 5-ALA and HAL present superior sensitivity compared to white light cystoscopy, 96, 97, and 73%, respectively. Nevertheless, the specificity is limited and does not significantly differ from white light cystoscopy, most likely due to the high false-positive rate [11]. However, Frimberger et al. [31] showed that with the addition of autofluorescence imaging to 5-ALA-induced fluorescence endoscopy for the detection of bladder carcinomas, the specificity increased from 67 to 88%, thereby reducing the false-positive rate.

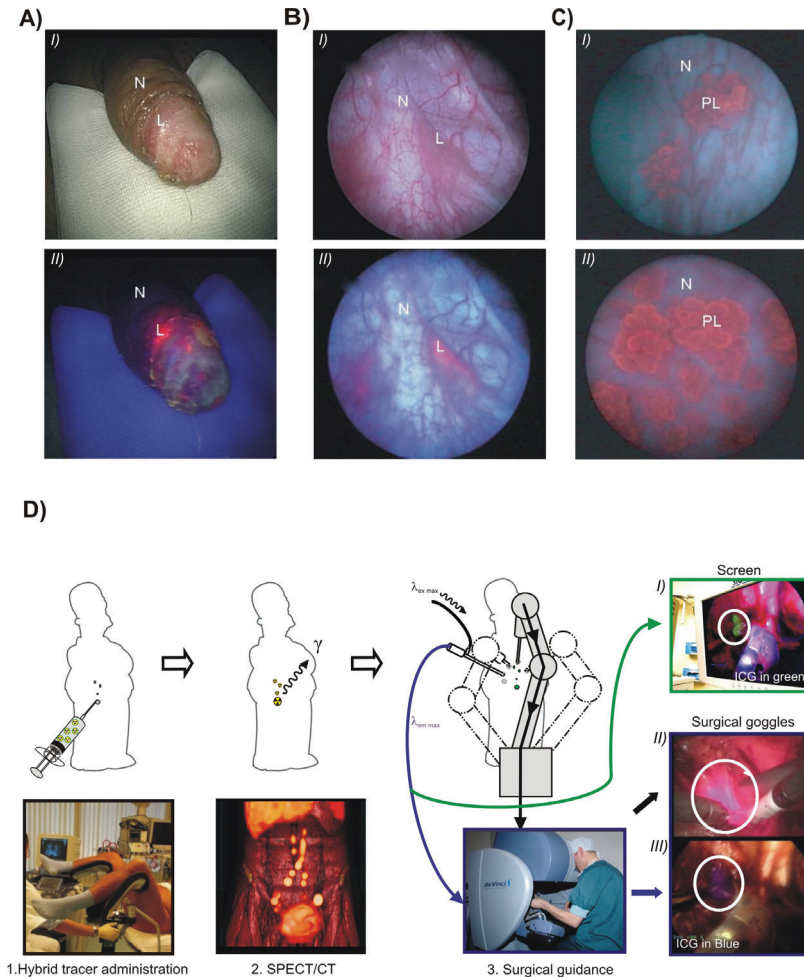


Figure 2. Clinical examples of implementation of fluorescence imaging during surgical procedures. A-C) White light images of the penis (AI) and bladder (BI and CI). Fluorescence imaging of PpIX (A, B) or hypericin (C) discriminated surgical margins of penile carcinoma (AII, L), carcinoma in situ of the bladder (BII, L) and papillary lesions in the bladder (CII, PL) from the normal tissue (N). Images were reprinted from Schlenker et al. [17], Ray et al. [8], and D'Hallewin et al. [24], respectively; D) Implementation of the hybrid tracer ICG-^{99m}Tc-nanocolloid during robot-assisted laparoscopic prostatectomy with SN biopsy procedure. Transrectal ultrasound-guided intra-

prostatic injection of the hybrid tracer (1). Preoperative SN identification with SPECT/CT (2). Intraoperative fluorescence-guided SN detection (3; I) Screen). The TilePro function of the da Vinci S surgical goggles allows simultaneous depiction of the three-dimensional surgical field and the intraoperative ICG-image (3; II) and III) Surgical goggles). Dotted lines highlight the fluorescent area. Images were reprinted from van der Poel et al. [1]. ICG = indocyanine green; L = lesion; N = normal tissue; PL = papillary lesion; SN = sentinel node; SPECT/CT = single photon emission computed tomography/computed tomography.

HYPERICIN

Hypericin (Planta Natural Products, Vienna, Austria) is a red fluorescing ($\lambda_{\text{ex max}}$: 598 nm; $\lambda_{\text{em max}}$: 649 nm) hydroxylated phenanthroprylene-quinone derivative present in plant of the genus *Hypericum* [32] with a very low quantum yield of less than 0.02 in water [33] (Table 1, Figure 1C). Hypericin as photosensitizer gives low systemic toxicity and accumulates usually in malignant tissue (Figure 2C) [26]. However, administration has been proven difficult due to its water insoluble properties. Recent clinical studies showed comparable sensitivity (82-94%), but increased specificity (91-94%) for the detection of bladder carcinoma as compared to 5-ALA and HAL [23-25] when hypericin was dissolved in ethanol and 1% plasma protein solution. Moreover, Kubin et al. [26] reported water soluble hypericin following polyvinylpyrrolidone (PVP) binding (Hypericin-PVP; Table 1, Figure 1D) for the detection of bladder cancer.

FLUORESCHEIN

Fluorescein (FLUORESCITE; Alcon Nederland B.V., Gorinchem, The Netherlands; Figure 1E) is an extremely bright synthetic dye with a quantum yield of 0.76 in water [34] that gives a visual yellow emission (530 nm) following excitation at 488 nm (Table 1). Although this emission is less than 700 nm, the yellow signal provides great contrast in the surgical field. Fluorescein as contrast agent combined with white light cystoscopy during confocal laser endomicroscopy of the bladder was shown to be able to distinguish normal and benign bladder epithelium from bladder carcinoma based on microscopic characteristics [18,19]. With fluorescein, which is considered a good imaging agent for angiography of the eye [35,36], Nguyen et al. [20] showed that the morphology of various intra-abdominal organs could be studied to distinguish diseased from normal tissue during urological interventions. Moreover, individual cells could also be visualized when fluorescein diffused into the interstitial space [20].

INDOCYANINE GREEN

The most widely applied near-infrared tracer is ICG (Pulsion Medical Systems, Munich, Germany; Figure 1F) with an emission in the 820-830 nm range following excitation at 780 nm (quantum yield 0.0028 in water [37]; Table 1). After intravenous injection, ICG binds rapidly to the plasma protein albumin (95%), which results in increased fluorescent properties (quantum yield 0.012 [37]), and a 25 nm red shift of the excitation maximum [37,38]. The emission signal of ICG is not visible with the naked eye and, therefore, a pseudo-color needs to be added. This color may significantly influence the contrast obtained in the surgical field; green provides a better contrast over a bloody background than red and is, therefore, often chosen. Moreover, in order to visualize the emission signal, a fluorescence camera system is required. ICG has a favorable safety profile with anaphylaxis occurring in less than 0.05% of cases.

Outside the field of urology, ICG is used for near-infrared fluorescence angiography [39-41]. Within the field of urology, Tanaka et al. [21] showed clear ureter visualization following retrograde injection of ICG. In addition, renal vasculature and tumors could be visualized during robot-assisted partial nephrectomy [22]. Tobis et al. [22] showed improved tumor detection in 11 patients with small renal masses following intravenous ICG injection. Here the vascular physiology of the tumor provided the diagnostic contrast. Although the short half-life of ICG (2-5 min) required repetitive injections, the recommended maximum dose of 2 mg/kg was not exceeded in any of the cases before resection of the tumor was completed [22]. Furthermore, ICG has found its application in the visualization of lymph vessels and leakage in patients with lymphedema [42].

ICG has most extensively been studied as an alternative for the more common vital dyes methylene blue and patent blue during intraoperative SN biopsy procedures in a variety of tumors such as skin, breast, gastrointestinal, anal, and lung cancer [42,43]. Intratumoral injection of ICG was shown to rapidly migrate to organ-associated lymph nodes that could be visualized via near-infrared fluorescence imaging [42,43]. The increased sensitivity obtained with near-infrared fluorescent tracers may allow for improved identification of lymph nodes at wavelengths not visible by the naked human eye. Binding of ICG to a protein, for example ICG-human serum albumin (ICG-HSA; Figure 1G) [44], increases the hydrodynamic diameter, and might thereby provide better retention and improved detection of the complex in the SNs [43]. Conventional preoperative SN visualization is done by injecting a ^{99m}Tc -labeled sulfur- or nanocolloid (HSA aggregate) to obtain optimal tracer accumulation at the landing sites after (intratumoral) injection. This enables preoperative planar lymphoscintigraphy and SPECT/CT imaging. Moreover, it allows for intraoperative localization of the SN using a gamma probe. The combination of ICG and ^{99m}Tc in the form of the hybrid tracer ICG- ^{99m}Tc -nanocolloid (Figure 1H) conveyed the nanocolloid properties to ICG and enabled intraoperative near-infrared imaging of the SNs in animal models for breast and prostate cancer [27,45]. Non-covalent self-assembly of ICG- ^{99m}Tc -nanocolloid by premixing ICG with ^{99m}Tc -nanocolloid, but not albumin, resulted in better accumulation in the (sentinel) lymph nodes, thereby increasing specificity [27,45]. The signal to background ratio was found to be superior over 'free' ICG and ICG-HSA. Recently, ICG- ^{99m}Tc -nanocolloid-based SN detection was also shown to be useful in prostate cancer patients [1]. This hybrid tracer allowed for preoperative detection of the SNs with SPECT/CT, whereas both the combination of the gamma probe and near-infrared fluorescence detection of ICG enabled intraoperative localization of the SNs (Figure 2D) [1]. Interestingly, following preoperative SPECT/CT imaging, four of 27 SNs were identified outside the extended pelvic lymph node dissection template, all of which were intraoperatively visualized via near-infrared fluorescence imaging [1]. A strong correlation was found between the radioactive and fluorescent contents in the excised lymph nodes indicating that the ICG- ^{99m}Tc -nanocolloid complex remained stable in the time period between injection and dissection of the nodes [1,27]. However, 15% of the SNs could not

be intraoperatively detected with fluorescence imaging alone due to the limited tissue penetration of the ICG fluorescent signal [1]. Especially in these instances, guidance to regions of interest by the radioactive component of the hybrid tracer is still desirable.

In summary, fluorescent tracers with visual emissions (PpIX, hypericin, fluorescein) suffer more from poor tissue penetration as compared to tracers with emissions in the near-infrared range. Because of its high quantum yield and therefore bright yellow emission signal, fluorescein can provide sufficient contrast over a bloody background as compared to dyes such as PpIX and hypericin that give a red fluorescence and have a low quantum yield. However, even with a low quantum yield, ICG provides good contrast over a bloody background. Other, the so-called hybrid tracers, may hold two different diagnostic labels for example a radioactive and a fluorescent label (e.g. ICG-^{99m}Tc-nanocolloid). These hybrid tracers are not only suitable for intraoperative fluorescence imaging, but also allow for integration of preoperative imaging using radioactive isotopes. This enables preoperative planning of the fluorescence-guided interventions.

FLUORESCENT IMAGING HARDWARE

The (human) body holds many other molecules that can also be excited by a light source. In order to be able to image the exogenous fluorescent tracer optimally, or to image a more specific endogenous fluorochrome, the excitation light is often tailored to the excitation maximum of the fluorescent tracer of interest by using light emitting diodes (LEDs) or lasers that only emit in a small wavelength region or by using specific band pass filters. Herein it is also important that reflection of the excitation light source does not contaminate the detected fluorescence signal. Using band pass filters in front of the charge coupled device (CCD) camera, collection of the emission signal can be limited to a specific region around the emission maximum of the fluorochrome. Although band pass filters block many of the background signals, it is seldom optimal. For this reason, most open clinical camera systems require darkening of the surgical field to prevent contamination by the surgical lights.

As Table 2 points out, roughly 14 imaging systems have been used in a clinical (urological) setting. Although hardware and software specifications for the individual systems vary significantly, most systems are optimized for near-infrared (ICG) imaging alone (Table 2). Most widely applied are the near-infrared imaging systems for open surgery. Applications using ICG vary from angiography to tumor resection margin imaging, SN detection, and visualization of lymphedema [42,43]. The PhotoDynamic Eye (PDE) system (Hamamatsu Photonics K.K., Hamamatsu, Japan), a commercially available handheld device, provides a black and white image of area of interest following excitation of the fluorochrome with 36 LEDs at 760 nm [46]. Other available near-infrared detection systems for open surgery are the SPY open surgery system (Novadaq Technologies, Concord, ON, Canada) [41], IC-View (Pulsion Medical Systems, Feldkirchen, Germany) [51], HyperEye (Mizuho Medical Co Ltd, Tokyo, Japan) [39], (mini-)FLARE (Beth Israel

Table 2. Clinically available imaging systems

System	Working distance	Excitation settings	Detection settings	Overlay on visual image	FOV	REF
<i>Open surgery systems</i>						
PDE	15-25 cm	36 LEDs; 760 nm	CCD camera; band pass filter >820 nm	NO	NS	[46]
SPY open surgery system	30 cm	Laser; 806 nm	CCD camera; >830 nm	NO	56 cm ²	[41]
HyperEye	30-50 cm	LED; 760 nm	CCD camera; non-Bayer color filters, 380-1200 nm (ICG: cut on filter >840 nm)	YES	76.5 cm ²	[39]
FLARE	45 cm	LED; 656-678 nm and 745-779 nm	CCD camera; band pass filter at 689-725 nm and 800-848 nm	YES	3.7-195 cm ²	[47]
Mini-FLARE	10-32 cm	LED; 656-678 nm and 745-779 nm	CCD camera; band pass filter at 689-725 nm and 800-848 nm	YES	<108 cm ²	[48]
FDPM	<76.2 cm	Laser diode; 785±10 nm	Notch filters at 785 and 830 nm	NO	<900 cm ²	[49]
SurgOptix	21 cm	Laser diode; 750 nm	CCD cameras; band pass filter 750±10 nm and 795±50 nm	YES	1.5-107 cm ²	[50]
IC-View	NS	Laser; 760 nm	CCD camera; >835 nm	NO		[51]
<i>Laparoscopic systems</i>						
D-light	NS	Xe light source; band pass filter 380-440nm	CCD camera; long wavelength filter >520nm	YES	NS	[52]
Olympus NBI	~3mm	Xe light source	CCD camera; 415±15nm, 540±10 nm and 600±10 nm	YES	NS	[53]
NIR D-light	NS	Xe light source; PpIX and ICG settings		NS	YES	NS [1]
NIR fluorescence for da Vinci Si surgical system	NS	Laser; 806nm		NS	NO	NS [22]
<i>Microscopy systems</i>						
Confocal laser endomicroscopy	NS	Laser; 488 nm	CCD camera; band pass filter at 530 nm	NS	NS	[20]
Multiphoton microscopy	NS	Ti-Sapphire laser; 780 nm	CCD camera; 380-530 nm	NS	NS	[54]

FOV = field of view; PDE = Photodynamic Eye; LED = light emitting diode; CCD = charge coupled device; NS = not specified; FLARE = fluorescence-assisted resection and exploration; FDPM = frequency-domain photon migration; PpIX = protoporphyrin IX; ICG = indocyanine green; NBI = narrow band imaging; NIR = near-infrared; Xe = xenon; Hg = mercury; Ti = titanium; and REF = reference.

Deaconess Hospital, Boston, MA, USA) [47,48], SurgOptix (Technical University Munich/Helmholtze Zentrum, Munich, Germany together with SurgOptix Inc., Redwood Shores, CA, USA) [50], and the FDPM system (Texas Medical Center, Houston, TX, USA) [49] (Table 2). SurgOptix and the (mini-)FLARE system also provide white light illumination of the surgical field. Moreover, by using more than one camera, these systems provide an overlay of the fluorescence and visual image. The Hyper Eye provides integration of the white light image with the near-infrared image.

With the rise of minimally invasive urologic interventions, endoscopic and/or laparoscopic systems will be of potential benefit. Currently, four systems are clinically available for laparoscopic fluorescence imaging, although development of new laparoscopic devices is ongoing [55,56]. Storz' D-light (KARL STORZ Endoskope GmbH & Co. KG, Tuttlingen, Germany) provides a system for both white light and collection of fluorescence in the visual emission range [52] and has found wide application for the detection of bladder cancer lesions following fluorescence imaging [2-11, 23-26, 29]. Moreover, Van der Poel et al. [1] used the near-infrared customized D-light system (KARL STORZ Endoskope GmbH & Co. KG) with incorporated near-infrared (ICG) settings for SN detection during robot-assisted laparoscopic prostatectomy procedures. Recently, Intuitive Surgical Inc. (Sunnyvale, CA, USA) introduced an integrated near-infrared imaging system for the da Vinci Si Surgical robot system in collaboration with Novadaq Technologies [22]. Lastly, Olympus Corp. introduced narrow band imaging (NBI) endoscopy in which the visual range emission band pass filters are set very narrow (Table 2). NBI allowed for detailed visualization of the mucosa surface, thereby distinguishing well-vascularized neoplastic lesions from normal bladder mucosa during cystoscopy procedures [53,57,58].

Of the near-infrared imaging systems, five imaging systems enable the detection of fluorochromes at various wavelengths. The customized near-infrared D-light system (KARL STORZ Endoskope GmbH & Co KG) provides both visual and near-infrared emission detection. With the (mini-)FLARE, fluorescence tracers can be excited between 656-678 and 745-779 nm after which emission light is collected via band pass filters from 689-725 and 800-848 nm, respectively [47,38]. SurgOptix provides emission collection using various CCD cameras with band pass filters at 795 ± 50 nm [50]. With the implementation of an extra band pass filter at 750 ± 10 nm, Themelis et al. [50] could perform light-absorption correction. The FDPM system provides Notch filters at 785 and 830 nm for the collection of the emission signal from the near-infrared fluorochrome [49].

Summarizing, the clinical availability of camera systems for fluorescent tracer imaging with emission in the visual range is limited, whereas a lot of research is ongoing in the development of imaging systems optimized for near-infrared dye imaging. Only a limited number of camera systems allows for multispectral imaging, among them the customized near-infrared D-light system (KARL STORZ Endoskope GmbH & Co KG). Although there are many systems available for open fluorescence-guided surgery, only a few laparoscopic devices are available for fluorescence imaging within the urological field.

FUTURE PERSPECTIVES IN FLUORESCENT TRACER DEVELOPMENT AND IMAGING SYSTEMS

The clinical tracers used to date provide merely the initial steps in fluorescence image-guided surgery. Targeting specific tumor markers with fluorescent tracers is expected to improve intraoperative imaging. Various tracers have been developed targeting the $\alpha\beta_3$ -integrin receptor which plays an important role in the process of (tumor) angiogenesis [59-62]. Moreover, enzyme-activatable tracers [61,63,64] might improve specificity of surgical guidance by making the contrast provided by the imaging agents dependent on local enzymatic activity of, for example, matrix metalloproteinases and cathepsins, which are frequently found to be overexpressed in prostate cancer cells [65]. Although we acknowledge the value of fluorescent tracers, in our opinion, the hybrid tracer approach is superior and therefore has the highest future potential. It enables the conversion of functional imaging (SPECT/CT and/or PET) data to the surgical theatre. Furthermore, it is possible to attach a fluorochrome and radioactive label to most targeting peptides, proteins, and/or antibodies, thereby creating targeted hybrid tracers. Of particular interest would be hybrid tracers for the most common biomarkers in urology. For example, for prostate cancer [65], wherein hybrid tracers have been developed preclinically for biomarkers such as chemokine receptor 4 [66], prostate specific membrane antigen [67], and integrins [66,68,69]. Nevertheless, for all these new compounds currently under development, obtaining clinical approval seems to be the biggest hurdle.

With the introduction of targeted and/or activatable (hybrid) tracers, more sophisticated imaging systems are desired to further improve the detectability of the fluorochromes. To date, most imaging systems are limited to the imaging of only one tracer. However, with the improvements in tracer development, one might think about developing imaging systems providing multispectral imaging. In this way, various fluorochromes can be used during the same procedure, possibly providing more specific imaging of the area of interest. Another interesting development in the field, and possibly applicable during urological interventions, was the introduction of confocal endomicroscopy (Table 2) for cellular structure visualization and vascularization imaging using fluorescein in order to improve surgical guidance [18-20]. Fluorescein, similarly to 'free' ICG, might also be of additional value for the detection of the SN following an intratumoral injection (F.W.B. van Leeuwen, unpublished observations). Moreover, multiphoton microscopy (Table 2) has been used to identify nerve structures based on tissue autofluorescence and might have the potential to improve the precision of nerve-sparing prostatectomy [54]. Lastly, Brouwer et al. described a navigation system for surgical guidance based on preoperative and intraoperatively acquired imaging data with the hybrid tracer ICG-^{99m}Tc-nanocolloid, thereby potentially improving the accuracy of fluorescence-guided surgery even further (Figure 3) [70].

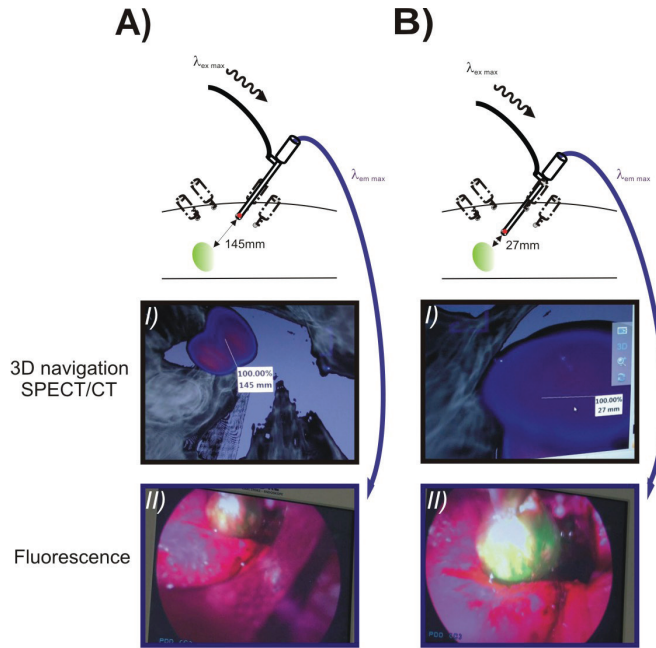


Figure 3. Image navigation towards the target lesion. Based on the preoperatively acquired SPECT/CT data (AI and BI), the laparoscope can be navigated toward the lesion. The navigation system provides the distance toward the lesion (dotted lines highlight the fluorescent area) in millimeters

in the schematic SPECT/CT based overview images, whereas the fluorescence laparoscope detects the fluorescent lesions (AII and BII). SPECT/CT = single photon emission computed tomography/computed tomography.

CONCLUSION

Fluorescence image-guided surgery holds promise for intraoperative identification of anatomical tumor structures within the field of urology. Currently, PpIX precursors 5-ALA and HAL, fluorescein, and ICG have received clinical FDA approval and are used for the identification of tumor locations and surgical tumor margins. Moreover, the hybrid tracer ICG-^{99m}Tc-nanocolloid was used for SN detection during robot-assisted laparoscopic prostatectomy. Challenges lie in the further optimization of targeted and/or activatable (hybrid) imaging agents and the integration between imaging agents and camera systems, thereby enabling more accurate fluorescence image guidance during surgical interventions.

REFERENCES

1. van der Poel HG, Buckle T, Brouwer OR, et al. Intraoperative laparoscopic fluorescence guidance to the sentinel lymph node in prostate cancer patients: clinical proof of concept of an integrated functional imaging approach using a multimodal tracer. *Eur Urol.* 2011;60:826-833.
2. Babjuk M, Soukup V, Petrik R, et al. 5-aminolaevulinic acid-induced fluorescence cystoscopy during transurethral resection reduces the risk of recurrence in stage Ta/T1 bladder cancer. *BJU Int.* 2005; 96:798-802.
3. Daniltchenko DI, Riedl CR, Sachs MD, et al. Long-term benefit of 5-aminolevulinic acid fluorescence assisted transurethral resection of superficial bladder cancer: 5-year results of a prospective randomized study. *J Urol.* 2005; 174:2129-2133.
4. Denzinger S, Burger M, Walter B, et al. Clinically relevant reduction in risk of recurrence of superficial bladder cancer using 5-aminolevulinic acid-induced fluorescence diagnosis: 8-year results of prospective randomized study. *Urology.* 2007; 69:675-679.
5. Filbeck T, Pichlmeier U, Knuechel R, et al. Clinically relevant improvement of recurrence-free survival with 5-aminolevulinic acid induced fluorescence diagnosis in patients with superficial bladder tumors. *J Urol.* 2002; 168:67-71.
6. Hermann GG, Mogensen K, Carlsson S, et al. Fluorescence-guided transurethral resection of bladder tumours reduces bladder tumour recurrence due to less residual tumour tissue in Ta/T1 patients: a randomized two-centre study. *BJU Int.* 2011; 108:E297-303.
7. Lerner SP, Liu H, Wu MF, et al. Fluorescence and white light cystoscopy for detection of carcinoma in situ of the urinary bladder. *Urol Oncol.* 2011;30:285-9.
8. Ray ER, Chatterton K, Khan MS, et al. Hexylaminolaevulinate fluorescence cystoscopy in patients previously treated with intravesical bacille Calmette-Guerin. *BJU Int.* 2010; 105:789-794.
9. Ray ER, Chatterton K, Thomas K, et al. Hexylaminolevulinate photodynamic diagnosis for multifocal recurrent nonmuscle invasive bladder cancer. *J Endourol.* 2009;23:983-988.
10. Stenzl A, Penkoff H, Dajc-Sommerer E, et al. Detection and clinical outcome of urinary bladder cancer with 5-aminolevulinic acid-induced fluorescence cystoscopy: a multicenter randomized, double-blind, placebo-controlled trial. *Cancer.* 2011;117:938-947.
11. Zaak D, Karl A, Knuchel R, et al. Diagnosis of urothelial carcinoma of the bladder using fluorescence endoscopy. *BJU Int.* 2005; 96:217-222.
12. Adam C, Salomon G, Walther S, et al. Photodynamic diagnosis using 5-aminolevulinic acid for the detection of positive surgical margins during radical prostatectomy in patients with carcinoma of the prostate: a multicentre, prospective, phase 2 trial of a diagnostic procedure. *Eur Urol.* 2009;55:1281-1288.

-
13. Fukuhara H, Inoue K, Satake H, et al. Photodynamic diagnosis of positive margin during radical prostatectomy: preliminary experience with 5-aminolevulinic acid. *Int J Urol*. 2011;18:585-591.
 14. Ganzer R, Blana A, Denzinger S, et al. Intraoperative photodynamic evaluation of surgical margins during endoscopic extraperitoneal radical prostatectomy with the use of 5-aminolevulinic acid. *J Endourol*. 2009;23:1387-1394.
 15. Zaak D, Sroka R, Khoder W, et al. Photodynamic diagnosis of prostate cancer using 5-aminolevulinic acid: first clinical experiences. *Urology*. 2008;72:345-348.
 16. Frimberger D, Schneede P, Hungerhuber E, et al. Autofluorescence and 5-aminolevulinic acid induced fluorescence diagnosis of penile carcinoma: new techniques to monitor Nd:YAG laser therapy. *Urol Res*. 2002;30:295-300.
 17. Schlenker B, Gratzke C, Seitz M, et al. Fluorescence-guided laser therapy for penile carcinoma and precancerous lesions: long-term follow-up. *Urol Oncol*. 2011; 29:788-793.
 18. Wu K, Liu JJ, Adams W, et al. Dynamic real-time microscopy of the urinary tract using confocal laser endomicroscopy. *Urology*. 2011;78:225-231.
 19. Sonn GA, Jones SN, Tarin TV, et al. Optical biopsy of human bladder neoplasia with in vivo confocal laser endomicroscopy. *J Urol* .2009; 182:1299-1305.
 20. Nguyen NQ, Biankin AV, Leong RW, et al. Real time intraoperative confocal laser microscopy-guided surgery. *Ann Surg*. 2009;249:735-737.
 21. Tanaka E, Ohnishi S, Laurence RG, et al. Real-time intraoperative ureteral guidance using invisible near-infrared fluorescence. *J Urol*. 2007;178:2197-2202.
 22. Tobis S, Knopf J, Silvers C, et al. Near infrared fluorescence imaging with robotic assisted laparoscopic partial nephrectomy: initial clinical experience for renal cortical tumors. *J Urol*. 2011; 186:47-52.
 23. D'Hallewin MA, De Witte PA, Waelkens E, et al. Fluorescence detection of flat bladder carcinoma in situ after intravesical instillation of hypericin. *J Urol*. 2000;164:349-351.
 24. D'Hallewin MA, Kamuhabwa AR, Roskams T, et al. Hypericin-based fluorescence diagnosis of bladder carcinoma. *BJU Int*. 2002;89:760-763.
 25. Sim HG, Lau WK, Olivo M, et al. Is photodynamic diagnosis using hypericin better than white-light cystoscopy for detecting superficial bladder carcinoma? *BJU Int*. 2005;95:1215-1218.
 26. Kubin A, Meissner P, Wierrani F, et al. Fluorescence diagnosis of bladder cancer with new water soluble hypericin bound to polyvinylpyrrolidone: PVP-hypericin. *Photochem Photobiol*. 2008;84:1560-1563.
 27. van Leeuwen AC, Buckle T, Bendle G, et al. Tracer-cocktail injections for combined pre and intraoperative multimodal imaging of lymph nodes in a spontaneous mouse prostate tumor model. *J Biomed Opt*. 2011;16:016004.
 28. Wachowska M, Muchowicz A, Firczuk M, et al. Aminolevulinic acid (ALA) as a product in photodynamic therapy of cancer. *Molecules*. 2011;16:4140-4164.

29. Celli JP, Spring BQ, Rizvi I, et al. Imaging and photodynamic therapy: mechanisms, monitoring, and optimization. *Chem Rev.* 2010;110:2795-2838.
30. Lozovaya GI, Masinovsky Z, Sivash AA. Protoporphyrin IX as a possible ancient photosensitizer: spectral and photochemical studies. *Orig Life Evol Biosph.* 1990;20:321-330.
31. Frimberger D, Zaak D, Stepp H, et al. Autofluorescence imaging to optimize 5-ALA-induced fluorescence endoscopy of bladder carcinoma. *Urology.* 2001;58:372-375.
32. Kubin A, Wierrani F, Burner U, et al. Hypericin: the facts about a controversial agent. *Curr Pharm Des.* 2005;11:233-253.
33. Wynn JL, Cotton TM. Spectroscopic properties of hypericin in solution and at surfaces. *J Phys Chem.* 1995;99:4317-4323.
34. Song A, Zhang J, Zhang M, et al. Spectral properties and structure of fluorescein and its alkyl derivatives in micelles. *Colloids and Surfaces A: Physiochem Eng Aspects.* 2000;167:253-262.
35. Bienfang DC, McKenna MJ, Papaliadis GN, et al. Case records of the Massachusetts General Hospital. Case 24-2011. A 36-year-old man with headache, memory loss, and confusion. *N Engl J Med.* 2011;365:549-559.
36. Spaide RF. Peripheral areas of nonperfusion in treated central retinal vein occlusion as imaged by wide-field fluorescein angiography. *Retina.* 2011;31:829-837.
37. Benson RC, Kues HA. Fluorescence properties of indocyanine green as related to angiography. *Phys Med Biol.* 1978;23:159-163.
38. Landsman ML, Kwant G, Mook GA, Zijlstra WG. Light-absorbing properties, stability, and spectral stabilization of indocyanine green. *J Appl Physiol.* 1976;40:575-583.
39. Handa T, Katare RG, Nishimori H, et al. New device for intraoperative graft assessment: HyperEye charge-coupled device camera system. *Gen Thorac Cardiovasc Surg.* 2010;58:68-77.
40. Sekijima M, Tojimbara T, Sato S, et al. An intraoperative fluorescent imaging system in organ transplantation. *Transplant Proc.* 2004;36:2188-2190.
41. Taggart DP, Choudhary B, Anastasiadis K, et al. Preliminary experience with a novel intraoperative fluorescence imaging technique to evaluate the patency of bypass grafts in total arterial revascularization. *Ann Thorac Surg.* 2003;75:870-873.
42. Polom K, Murawa D, Rho YS, et al. Current trends and emerging future of indocyanine green usage in surgery and oncology: a literature review. *Cancer.* 2011;117:4812-4822.
43. Schaafsma BE, Mieog JS, Hutteman M, et al. The clinical use of indocyanine green as a near-infrared fluorescent contrast agent for image-guided oncologic surgery. *J Surg Oncol.* 2011;104:323-332.
44. Hutteman M, Mieog JS, van der Vorst JR, et al. Randomized, double-blind comparison of indocyanine green with or without albumin premixing for near-infrared fluorescence imaging of sentinel lymph nodes in breast cancer patients. *Breast Cancer Res Treat.* 2011;127:163-170.

-
45. Buckle T, van Leeuwen AC, Chin PT, et al. A self-assembled multimodal complex for combined pre and intraoperative imaging of the sentinel lymph node. *Nanotechnology*. 2010;21:355101.
 46. Unno N, Inuzuka K, Suzuki M, et al. Preliminary experience with a novel fluorescence lymphography using indocyanine green in patients with secondary lymphedema. *J Vasc Oncol*. 2007;45:1016-1021.
 47. Troyan SL, Kianzad V, Gibbs-Strauss SL, et al. The FLARE intraoperative near-infrared fluorescence imaging system: a first-in-human clinical trial in breast cancer sentinel lymph node mapping. *Ann Surg Oncol*. 2009;16:2943-2952.
 48. Mieog JS, Troyan SL, Hutteman M, et al. Toward optimization of imaging system and lymphatic tracer for near-infrared fluorescent sentinel lymph node mapping in breast cancer. *Ann Surg Oncol*. 2011;18:2483-2491.
 49. Sevick-Muraca EM, Sharma R, Rasmussen JC, et al. Imaging of lymph flow in breast cancer patients after microdose administration of a near-infrared fluorophore: feasibility study. *Radiology*. 2008;246:734-741.
 50. Themelis G, Yoo JS, Soh KS, et al. Real-time intraoperative fluorescence imaging system using light-absorption correction. *J Biomed Opt*. 2009;14:064012.
 51. Hirche C, Murawa D, Mohr Z, et al. ICG fluorescence-guided sentinel node biopsy for axillary nodal staging in breast cancer. *Breast Cancer Res Treat*. 2010;121:373-378.
 52. Riedl CR, Plas E, Pfluger H. Fluorescence detection of bladder tumors with 5-amino-levulinic acid. *J Endourol*. 1999;13:755-759.
 53. Kuznetsov K, Lambert R, Rey JF. Narrow-band imaging: potential and limitations. *Endoscopy*. 2006;38:76-81.
 54. Yadav R, Mukherjee S, Hermen M, et al. Multiphoton microscopy of prostate and periprostatic neural tissue: a promising imaging technique for improving nerve-sparing prostatectomy. *J Endourol*. 2009;23:861-867.
 55. Matsui A, Tanaka E, Choi HS, et al. Real-time intra-operative near-infrared fluorescence identification of the extrahepatic bile ducts using clinically available contrast agents. *Surgery*. 2010;148:87-95.
 56. van der Pas MH, van Dongen GA, Cailler F, et al. Sentinel node procedure of the sigmoid using indocyanine green: feasibility study in a goat model. *Surg Endosc*. 2010;24:2182-2187.
 57. Herr HH. Narrow band imaging cystoscopy. *Urol Oncol*. 2011;29:353-357.
 58. Shen YJ, Zhu YP, Ye DW, et al. Narrow-band imaging flexible cystoscopy in the detection of primary nonmuscle invasive bladder cancer: a 'second look' matters? *Int Urol Nephrol*. 2011;44:451-457.
 59. Hutteman M, Mieog JS, van der Vorst JR, et al. Intraoperative near-infrared fluorescence imaging of colorectal metastases targeting integrin $\alpha(v)\beta(3)$ expression in a syngeneic rat model. *Eur J Surg Oncol*. 2011;37:252-257.

60. Mery E, Jouve E, Guillermet S, et al. Intraoperative fluorescence imaging of peritoneal dissemination of ovarian carcinomas. A preclinical study. *Gyn Oncol.* 2011;122:155-162.
61. Penna FJ, Freilich DA, Alvarenga C, Nguyen HT. Improving lymph node yield in retroperitoneal lymph node dissection using fluorescent molecular imaging: a novel method of localizing lymph nodes in Guinea pig model. *Urology.* 2011;78:232e15-232e18.
62. Themelis G, Harlaar NJ, Kelder W, et al. Enhancing surgical vision by using real-time imaging of avb3-Integrin targeted near-infrared fluorescent agent. *Ann Surg Oncol.* 2011;18:3506-3513.
63. Liu Y, Bauer AQ, Akers WJ, et al. Hands-free, wireless goggles for near-infrared fluorescence and real-time image-guided surgery. *Surgery.* 2011;149:689-698.
64. Mieog JS, Hutteman M, van der Vorst JR, et al. Image-guided tumor resection using real-time near-infrared fluorescence in a syngeneic rat model of primary breast cancer. *Breast Cancer Res Treat.* 2011;128:679-689.
65. Yang SY, Adelstein J, Kassis AI. Putative molecular signatures for the imaging of prostate cancer. *Expert Rev Mol Diagn.* 2010;10:65-74.
66. Kuil J, Velders AH, van Leeuwen FW. Multimodal tumor-targeting peptides functionalized with both a radio- and a fluorescent label. *Bioconjug Chem.* 2010; 21:1709-1719.
67. Banerjee SR, Pullambhatla M, Byun Y, et al. Sequential SPECT and optical imaging of experimental models of prostate cancer with a dual modality inhibitor of the prostate-specific membrane antigen. *Angew Chem Int Ed Engl.* 2011;50:9167-9170.
68. Edwards WB, Akers WJ, Ye Y, et al. Multimodal imaging of integrin receptor-positive tumors by bioluminescence, fluorescence, gamma scintigraphy, and single-photon emission computed tomography using a cyclic RGD peptide labeled with a near-infrared fluorescent dye and a radionuclide. *Mol Imaging.* 2009;8:101-110.
69. Li C, Wang W, Wu Q, et al. Dual optical and nuclear imaging in human melanoma xenografts using a single targeted imaging probe. *Nucl Med Biol.* 2006;33:349-358.
70. Brouwer OR, Buckle T, Bunschoten A, et al. Image navigation as a mean to expand the boundaries of fluorescence-guided surgery. *Phys Med Biol.* 2012;57:3123-36.

SUPPORTING INFORMATION

PRINCIPLE OF FLUORESCENCE

The process of fluorescence can be divided into three steps: 1) Excitation of the molecule by photons; 2) Internal conversion; and 3) Emission of photons. This process is graphically represented in a Jablonski diagram (Figure SI 1A; for more detailed information see Ruggi et al. [1]). Each fluorochrome has its own particular excitation ($\lambda_{\text{ex max}}$) and emission maximum ($\lambda_{\text{em max}}$) (Table 1). However, the excitation and emission signals are often very broad (Figure SI1B). In fluorescence imaging this means that you need both a light source matching the excitation maximum of the fluorochrome and a camera system for the detection of the emission light around the emission maximum peak. In general, emissions are classified in visual emissions with a wavelength of 400-650 nm, far-red emissions (650-700 nm), and the by eye invisible near-infrared emissions 700-1000 nm (Figure SI 1C). The efficacy through which this photon emission occurs for a particular molecule is depicted by the fluorescence quantum yield (ranging from 0-1) of the fluorochrome.

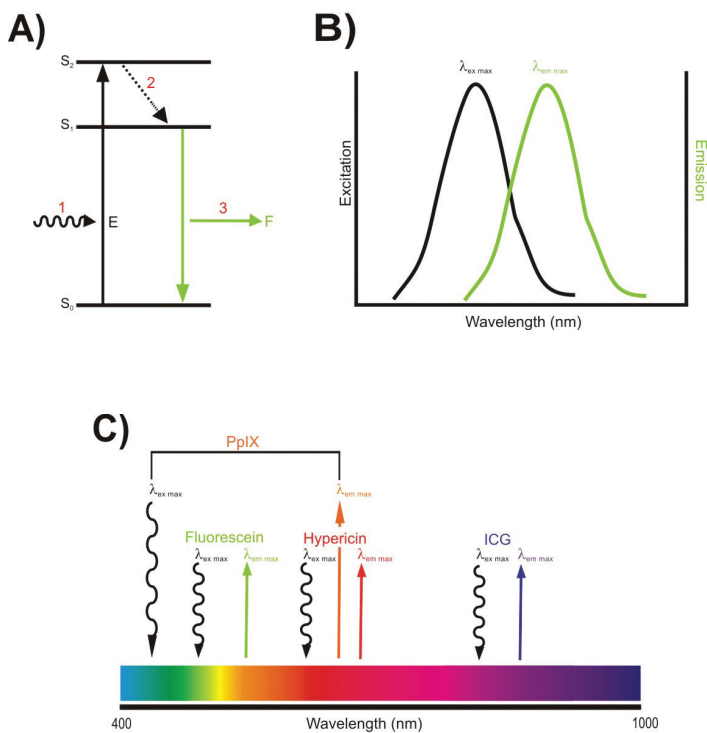


Figure SI1. Basics of fluorescence. A) Jablonski diagram of the process of fluorescence: 1. Excitation of the molecule by photons (E); 2. Internal conversion; and 3. Emission of photons (F). S_0 , S_1 and S_2 depict the various energy levels; B) Schematic overview of a general excitation and emission spectrum of a fluorochrome where $\lambda_{\text{ex max}}$ = excitation maximum and $\lambda_{\text{em max}}$ = emission maximum; and C) Light spectrum with $\lambda_{\text{ex max}}$ and $\lambda_{\text{em max}}$ of various fluorochromes. PpIX = protoporphyrin IX; and ICG = indocyanine green.

Absorption and/or light scatter by tissues limits the penetration of the excitation light and thus the depth at which fluorochromes can be excited. For the fluorescent emissions, the surrounding tissues also cause signal attenuation via absorbance and/or scattering. The major absorbers of visible light are native fluorescent molecules such as oxy- and deoxyhemoglobin in blood, whereas lipids and water are the major absorbers of infrared light at wavelengths >1000 nm [2-4]. Scattering may also occur via these molecules, but tissue architecture and intracellular composition (organelle density) are also of influence [2, 3]. Combined, the depth at which a fluorescent signal can be detected is limited, even in the most optimal near-infrared wavelength window. Signal penetration varies from millimeters (visual emissions 450-650 nm) to centimeters for near-infrared emissions [5, 6]. Moreover, tissue autofluorescence (endogenous fluorescence) may impair the specificity of detection [6]. In the process of autofluorescence, naturally occurring tissue fluorophores generally emit light <700 nm when excited by a light source [3]. Throughout the body, autofluorescence can be caused by various molecules such as nicotinamide (NAD[H]) and flavins. The extracellular matrix can also contribute to autofluorescence due to the intrinsic properties of collagen and elastin [2, 7].

REFERENCES

1. Ruggi A, van Leeuwen FW, Velders AH. Interaction of dioxygen with the electronic excited state of Ir(III) and Ru(II) complexes: Principles and biomedical applications. *Coord Chem Rev.* 2011;21-22:2542-2554.
2. Bremer C, Ntziachristos V, Weissleder R. Optical-based molecular imaging: contrast agents and potential medical applications. *Eur Radiol.* 2003;13:231-43.
3. Klohs J, Wunder A, Licha K. Near-infrared fluorescent probes for imaging vascular pathophysiology. *Basic Res Cardiol.* 2008;103:144-51.
4. Weissleder R, Ntziachristos V. Shedding light onto live molecular targets. *Nat Med.* 2003;9:123-8.
5. Buckle T, Chin PT, van den Berg NS et al., Tumor bracketing and safety margin estimation using multimodal marker seeds: a proof of concept. *J Biomed Opt.* 2010;15: 056021.
6. Chin PT, Buckle T, Aguirre de Miguel A et al., Dual-emissive quantum dots for multispectral intraoperative fluorescence imaging. *Biomaterials.* 2010;31:6823-32.
7. Frimberger D, Zaak D, Stepp H et al. Autofluorescence imaging to optimize 5-ALA-induced fluorescence endoscopy of bladder carcinoma. *Urology.* 2001;58:372-5.